Haverford College

Haverford Scholarship

2011

The Sloan Digital Sky Survey Data Release 7 Spectroscopic M Dwarf Catalog. II. Statistical Parallax Analysis

John J. Bochanski
Haverford College, jbochans@haverford.edu

Suzanne L. Hawley

Andrew A. West

Follow this and additional works at: https://scholarship.haverford.edu/astronomy_facpubs

Repository Citation

THE SLOAN DIGITAL SKY SURVEY DATA RELEASE 7 SPECTROSCOPIC M DWARF CATALOG. II. STATISTICAL PARALLAX ANALYSIS

JOHN J. BOCHANSKI[1,2], SUZANNE L. HAWLEY[3], AND ANDREW A. WEST[4,5]
[1] Astronomy and Astrophysics Department, Pennsylvania State University, 525 Davey Laboratory, University Park, PA 16802, USA; jjb29@psu.edu
[2] Kavli Institute for Astrophysics and Space Research, Massachusetts Institute of Technology, Building 37, 77 Massachusetts Avenue, Cambridge, MA 02139, USA
[3] Astronomy Department, University of Washington, Box 351580, Seattle, WA 98195, USA
[4] Department of Astronomy, Boston University, 725 Commonwealth Avenue, Boston, MA 02215, USA

ABSTRACT

We present a statistical parallax analysis of low-mass dwarfs from the Sloan Digital Sky Survey. We calculate absolute r-band magnitudes (M_r) as a function of color and spectral type and investigate changes in M_r with location in the Milky Way. We find that magnetically active M dwarfs are intrinsically brighter in M_r than their inactive counterparts at the same color or spectral type. Metallicity, as traced by the proxy ζ, also affects M_r, with metal-poor stars having fainter absolute magnitudes than higher metallicity M dwarfs at the same color or spectral type. Additionally, we measure the velocity ellipsoid and solar reflex motion for each subsample of M dwarfs. We find good agreement between our measured solar peculiar motion and previous results for similar populations, as well as some evidence for differing motions of early and late M-type populations in U and W velocities that cannot be attributed to asymmetric drift. The reflex solar motion and the velocity dispersions both show that younger populations, as traced by magnetic activity and location near the Galactic plane, have experienced less dynamical heating. We introduce a new parameter, the independent position altitude (IPA), to investigate populations as a function of vertical height from the Galactic plane. M dwarfs at all types exhibit an increase in velocity dispersion when analyzed in comparable IPA subgroups.

Key words: Galaxy: kinematics and dynamics – methods: statistical – solar neighborhood – stars: fundamental parameters – stars: kinematics and dynamics – stars: low-mass

Online-only material: color figures

1. INTRODUCTION

Low-mass dwarfs ($0.08\,\mathcal{M}_\odot < \mathcal{M} < 0.8\,\mathcal{M}_\odot$) dominate the stellar content of the Milky Way (Bochanski et al. 2010). However, the study of these stars in large numbers was only recently realized with the advent of surveys such as the Sloan Digital Sky Survey (SDSS; York et al. 2000) and the Two Micron All Sky Survey (2MASS; Skrutskie et al. 2006). These surveys with their precise, multi-band photometry and (in the case of SDSS) spectroscopic coverage have led to observational catalogs of unprecedented size. Currently, the largest spectroscopic database of M dwarfs (West et al. 2011, hereafter Paper I) has produced spectral types, radial velocities (RVs), and chromospheric activity estimates (as traced by Balmer series emission) for over 70,000 M dwarfs. SDSS photometry of millions of stars has been used to measure the field luminosity and mass functions of M dwarfs (Covey et al. 2008; Bochanski et al. 2010), the structure of the Milky Way's thin and thick disks (Jurić et al. 2008; Bochanski et al. 2010), and the properties of wide, common proper motion binaries (Dhital et al. 2010).

The ubiquity and long main-sequence lifetimes of low-mass stars (Laughlin et al. 1997) make M dwarfs ideal tracers of nearby Galactic structure and kinematics (e.g., Reid & Majewski 1993; Reid et al. 1995; Bochanski et al. 2007a, 2010; Fuchs et al. 2009). Despite the recent advances enabling the study of these stars in a broad Galactic context, one fundamental parameter remains elusive: distance. Accurate trigonometric parallaxes, and the resulting absolute magnitude

and distance measurements, remain difficult to obtain due to the intrinsic faintness ($L \lesssim 0.05\,L_\odot$) of low-mass stars. The largest trigonometric parallax survey to date was performed by the *Hipparcos* satellite (ESA 1997; van Leeuwen 2007). However, due to the relatively bright magnitude limit of the *Hipparcos* sample ($V \lesssim 12$), M dwarfs observed by *Hipparcos* are saturated in SDSS photometry, hindering the construction of a color–absolute-magnitude relation (CMR) in native SDSS filters. A few parallax estimates of SDSS M dwarfs have been obtained (e.g., Dahn et al. 2002; Vrba et al. 2004), but these measurements are observationally taxing and take years to complete, and are thus limited in number ($\sim$20). Current (Lépine et al. 2009; Riedel et al. 2010; Smart et al. 2010; J. K. Faherty 2010, private communication) and future parallax studies, such as *GAIA* (Perryman et al. 2001), will add valuable observations to this regime.

Since trigonometric parallaxes for the vast majority of SDSS M dwarfs are not available, alternate means to estimate their absolute magnitudes must be employed. Hawley et al. (2002) and West et al. (2005) used SDSS–2MASS cross-matching to create M_J–spectral-type relations, and combined with average colors as a function of spectral type, to construct SDSS CMRs. D. A. Golimowski et al. (2008, private communication) and Bochanski (2008) used $u'g'r'i'z'$ photometry of $\sim$200 nearby M dwarfs with accurate trigonometric parallaxes, and transformed from the $u'g'r'i'z'$ system of the SDSS photometric telescope to the native SDSS $ugriz$ system using the relations of Davenport et al. (2007). Other CMRs applicable for warmer stars in the SDSS filter set have been derived using binaries (Sesar et al. 2008) and averages of existing CMRs (Jurić et al. 2008). Using a kinematic model for motions of stars

---

[5] Visiting Investigator, Department of Terrestrial Magnetism, Carnegie Institute of Washington, 5241 Broad Branch Road, NW, Washington, DC 20015, USA.

in the Milky Way, Bond et al. (2010) derived a distance scale and CMR for main-sequence stars observed by SDSS. Other studies have used 2MASS–SDSS color transformations (Bilir et al. 2009) and synthetic photometry (Covey et al. 2007) to derive CMRs in the *ugriz* filter system.

One method for constructing CMRs in the native SDSS system that has not yet been utilized is the classical statistical parallax method. Using proper motions and RVs of a large number stars from a homogeneous population, an estimate of the average absolute magnitude, the velocity ellipsoid, and the Sun's peculiar motion can be obtained. This method has a rich history in the astronomical literature (e.g., van Herk 1965; Clube & Jones 1971; Murray 1983; Popowski & Gould 1998) and has previously been employed for RR Lyraes (e.g., Hawley et al. 1986; Strugnell et al. 1986; Layden et al. 1996; Fernley et al. 1998; Popowski & Gould 1998) and Cepheids (e.g., Wilson et al. 1991).

In addition to absolute magnitude estimates, the statistical parallax technique provides a measurement of the velocity ellipsoid of the stellar population and the reflex motion of the Sun. The velocity ellipsoid is described by dispersions and directions along three principal axes. Low-mass stars make excellent tracers of the local Galactic potential (Reid et al. 1997; Bochanski et al. 2007a; Fuchs et al. 2009) as constrained by the observed velocity dispersions. The solar peculiar motion determination complements studies using *Hipparcos* proper motions of nearby, young stars (Dehnen & Binney 1998), SDSS observations of M dwarfs (Fuchs et al. 2009), and the Palomar-Michigan State University survey of nearby M dwarfs (PMSU; Reid et al. 1995; Hawley et al. 1996).

In this paper, we use the large spectroscopic sample of M dwarfs described in Paper I to determine absolute magnitudes in the native SDSS filters and examine kinematics using the statistical parallax method. The observations employed in our study are described in Section 2. We detail our statistical parallax analysis in Section 3. Our results are presented in Section 4, with conclusions following in Section 5.

2. OBSERVATIONS

Accurate and precise photometry, astrometry, and velocities are required for statistical parallax analysis. The data were obtained from the latest SDSS data release (DR7; Abazajian et al. 2009) which contains photometry over nearly 10,000 deg^2 down to faint magnitudes ($r \sim 22$) in five filters (*ugriz*; Fukugita et al. 1996). When sky conditions at Apache Point Observatory were not photometric, the SDSS operated in a spectroscopic mode. SDSS photometry was used to target objects for spectroscopic follow-up, primarily galaxies (Strauss et al. 2002) and quasars (Richards et al. 2002). Approximately 460,000 stellar spectra were also obtained both as targeted and serendipitous observations. Twin fiber-fed spectrographs collected 640 observations simultaneously, with individual 15–20 minute exposures being co-added for a typical total exposure time of ∼45 minutes. These medium-resolution ($R \sim 2000$) spectra cover the entire optical bandpass (3800–9200 Å).

The absolute astrometric precision of SDSS is <0″.1 in each coordinate (Pier et al. 2003). Proper motions for SDSS objects were calculated by matching to the USNO-B survey (Munn et al. 2004, 2008). The proper motions have a baseline of ∼50 years and a typical precision of ∼3 mas yr^{-1} in right ascension and declination.

In Paper I, we described the SDSS DR7 spectra that we compiled into the largest spectroscopic catalog of M dwarfs

Table 1
Statistical Parallax Fit Parameters

Parameter	Units	Description
σ_U	km s^{-1}	Velocity dispersion in radial direction
σ_V	km s^{-1}	Velocity dispersion in orbital direction
σ_W	km s^{-1}	Velocity dispersion in vertical direction
r, ϕ, z	radians	Orientation of velocity ellipsoid
U	km s^{-1}	Solar peculiar motion (r)
V	km s^{-1}	Solar peculiar motion (ϕ)
W	km s^{-1}	Solar peculiar motion (z)
k	. . .	Distance scale
σ_k	. . .	Dispersion in distance scale

ever constructed, containing ∼70,000 stars. Briefly, the catalog was obtained by color selection of stars with $r - i > 0.42$ and $i - z > 0.24$, before correcting for Galactic reddening (Schlegel et al. 1998). Each star was processed with the Hammer IDL package (Covey et al. 2007). The Hammer provides spectral-type estimates and measures a number of spectral features, including Hα equivalent width and various TiO and CaH band head strengths. Each spectrum was then visually inspected and non-M dwarf contaminants were culled from the catalog. Spectral types were determined by comparing to the SDSS templates (Bochanski et al. 2007b). The RVs were measured by cross-correlating each spectrum with the appropriate template from Bochanski et al. (2007b), with a precision of ∼7 km s^{-1}. See Paper I for more detailed information about the selection and characteristics of the DR7 catalog.

For the sample used in the statistical parallax analysis, we required that stars have well-measured proper motions and radial velocities, and precise photometry (see Bochanski et al. 2010 for information on photometric flag cuts and Dhital et al. 2010 for our kinematic quality flags). Our quality cuts reduced the original sample to 40,963 stars.

3. METHOD

We employed the maximum likelihood formulation of classical statistical parallax analysis as presented by Murray (1983) and used previously to analyze RR Lyrae stars (Hawley et al. 1986; Strugnell et al. 1986; Layden et al. 1996; Fernley et al. 1998) and Cepheids (Wilson et al. 1991). A variation of the model was used to investigate the kinematics of the nearby M dwarfs from the PMSU sample (Hawley et al. 1996). Briefly, this statistical parallax method models the velocity distribution of a homogeneous stellar population with nine kinematic parameters, including the three velocities of the reflex solar motion, and the three directions and three dispersions of the velocity ellipsoid, which describes the random and peculiar velocities of the population. The stars are assumed to have an absolute magnitude with some intrinsic dispersion, and these two additional parameters determine the distance used to transform the observed proper motions into transverse velocities. The 11 parameters used in the model are described in Table 1.

The observational data needed for the analysis are the position, apparent magnitude (corrected for Galactic extinction), proper motions, and RV for each star in the sample. The uncertainties in the data are used to assign appropriate weights in the solution. We solved for the 11 parameters in the model simultaneously by maximizing the likelihood using geometric simplex optimization (Nelder & Mead 1965; Daniels 1978). Uncertainties in the parameters were determined by numerical computation of the derivative of each parameter individually,

Table 2
SDSS Subsamples

Initial Cut	Bin Size	Further Criteria	Comments
Spectral type	1 type bins	...	...
Color	0.3 mag bins	...	...
		Activity	Hα active stars defined in Paper I
		Hemisphere	N and S Galactic Hemispheres
		ζ	0.25 bins
		IPA	10 bins per spectral type
		Distance	<500 pc & <700 pc

Notes. Bins with fewer than 100 stars were not used in this analysis.

while keeping all other parameters fixed. The maximum likelihood equations and simplex method are described in detail in Hawley et al. (1986).

With any multi-parameter fit, sensible constraints are necessary to ensure that the model does not prefer an unrealistic portion of χ^2 space. For this analysis, we fixed one parameter, σ_k. This parameter is related to the spread in absolute magnitude, σ_M, by the following equation from Hawley et al. (1986):

$$\sigma_M{}^2 = \log_{10}\left[1 + \sigma_k^2/(1+k)^2\right]/(0.04 \ln 10), \qquad (1)$$

where σ_M is the spread in absolute magnitude for a given luminosity bin and σ_k is the spread in k which is a distance scale parameter. The absolute magnitude is related to k through the following equation:

$$M_r = 5 \log_{10}(1+k) + M_A - 0.1 \ln 10 (\sigma_M)^2, \qquad (2)$$

where M_A is an initial estimate of the absolute magnitude. We fixed σ_k at four values: 0.05, 0.1, 0.2, and 0.3. Usually $k \sim 0.01$–0.02, so $\sigma_k = 0.2$ corresponds to $\sigma_M \sim 0.4$ which is the typical dispersion in absolute magnitude for low-mass stars (Bochanski et al. 2010).

3.1. Constructing Subsamples for Analysis

Our spectroscopic sample is much larger than was available for previous statistical parallax studies, which contained observations of a few hundred or less objects. Thus, we were able to divide the sample into smaller subsamples, selected on color, spectral type, magnetic activity (as traced by Hα), metallicity (using the ζ parameter of Lépine et al. 2007), position on the sky (northern and southern Galactic hemispheres), distance (estimated from the M_r, $r - z$ CMR relation from Bochanski et al. 2010), and Galactic height (discussed further below). We required at least 100 stars in each subsample to ensure a meaningful solution. Table 2 lists the properties of the various subsamples.

The color, spectral type, metallicity, and magnetic activity subsamples were chosen to explore intrinsic variations within the M dwarf population, as traced by their absolute magnitudes and kinematics. The position and distance subsets were examined to ensure that we were not biased by extinction or proper motion limits. While the majority of our sample is contained at high Galactic latitudes ($b \sim 50°$) in low extinction regions (the median extinction in r is 0.07 mag), some sightlines to the south (through the Plane) may be affected by extinction and reddening. Current efforts to model the three-dimensional dust distribution within the SDSS footprint (D. Jones et al. 2010, private communication) will improve the extinction and reddening estimates for these stars.
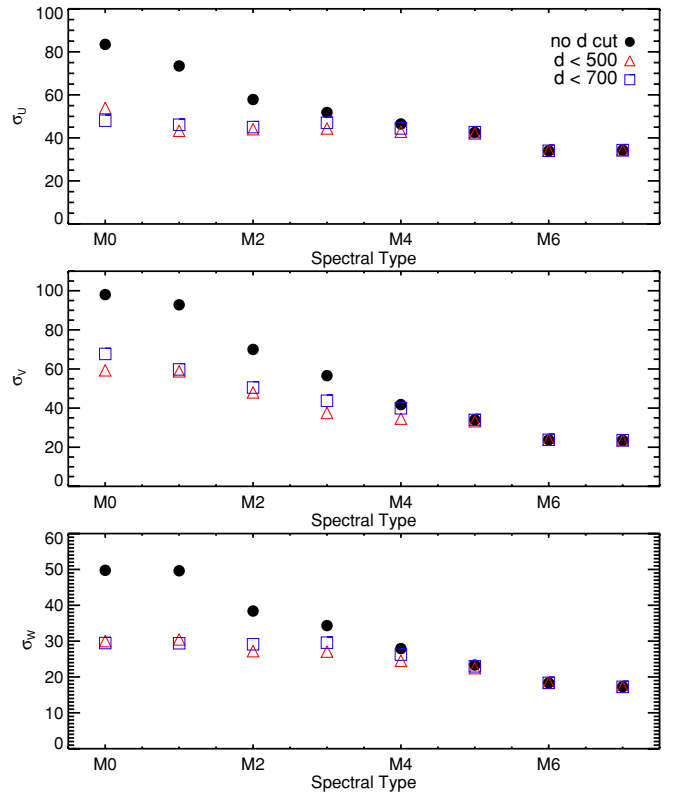
Figure 1. *UVW* dispersions vs. spectral type for $d < 500$ pc (open triangles), $d < 700$ pc (open squares), and no distance limit (filled circles). Including more distant stars beyond our proper motion precision limit artificially inflates the measured dispersions for early-type stars.

(A color version of this figure is available in the online journal.)

Our proper motion catalog, described in Munn et al. (2004, 2008), has a precision limit of 3 mas yr^{-1}. For a typical thin disk star with a transverse velocity of ~ 10 km s^{-1}, this limit corresponds to a limiting distance of ~ 700 pc. Beyond this distance, only stars with larger transverse motions would be measured with precise proper motions, artificially biasing the measured velocity dispersion. Thus, two distance limits were explored: stars with $d < 500$ pc and $d < 700$ pc. The 500 pc cut corresponds to a more conservative estimate of the proper motion precision. The effects of these distance limits are shown in Figure 1. Early-type M dwarfs, which are found at larger distances, are biased toward larger velocity dispersions if a distance limit is not enforced. The 500 pc and 700 pc limits give similar results, so we adopt a $d < 700$ pc limit for the remainder of this study. Further kinematic analysis is discussed in Section 4.2. The $d < 700$ pc cut limits the total number of stars in our sample to 22,542. In Table 3, we report the median, minimum, and maximum heights above the Plane for the stars in our $d < 700$ pc sample. The heights were measured using distances from the M_r, $r - z$ CMR of Bochanski et al. (2010).

Finally, to probe changes in the kinematics and absolute magnitude as a function of height in the Milky Way disk, we divided each spectral type and color bin according to the independent position altitude (IPA). At a given spectral type, bins in apparent magnitude will correspond to spherical shells in space. The IPA cuts are slices in Galactic height, defined as

$$\mathrm{IPA} \equiv 10^{m_r/5} \sin b, \qquad (3)$$

where m_r is the observed r-band magnitude and b is the Galactic latitude of the star. We stress that the IPA can only be used for

Table 3
Galactic Heights of SDSS M Dwarfs

	Median Height	Min. Height	Max Height	N_{Stars}
Spectral Type				
M0	395	20	690	1323
M1	392	22	689	1877
M2	337	11	693	4700
M3	274	14	712	6156
M4	214	9	694	4784
M5	137	9	694	1616
M6	108	4	423	1333
M7	82	0	230	753
$r-z$				
0.75	402	20	690	348
1.05	395	23	688	1647
1.35	375	16	693	2914
1.65	309	11	712	5937
1.95	254	13	694	5639
2.25	181	9	634	2922
2.55	123	11	387	818
2.85	118	7	304	958
3.15	98	0	221	960
3.45	76	2	340	296
3.75	58	5	126	102

Notes. All heights reported in pc and measured using distances from the M_r, $r-z$ CMR of Bochanski et al. (2010).

relative comparisons within the same intrinsic luminosity bins. That is, M0 and M6 stars with the same IPA value will be located at very different Galactic heights. The IPA is useful as it avoids the assumption of an absolute magnitude, allowing an independent determination for each IPA subset. It is based entirely on observable properties and is somewhat analogous to the often-used reduced proper motion (Luyten 1925).

3.2. Computational Method

Following the method of Hawley et al. (1986), each subsample of M dwarfs was analyzed using the following prescription. Ten runs were calculated for each data set. The initial absolute magnitude estimates were derived from the M_r, $r-z$ CMR of Bochanski et al. (2010). The absolute magnitude estimate was updated after each run, with the output of the previous run being used as input for the next. For a given run, the simplex optimization iterated 5000 times. Thus, for each subsample, 50,000 iterations were computed. This ensured that the simplex operator had sufficient freedom to explore parameter space and converged to the best (maximum likelihood) answer. Typically, convergence was obtained after 25,000 iterations.

4. RESULTS

The results of our analysis are detailed below. The outputs from the code returned three major results: the absolute magnitude of a given stellar sample, the Sun's velocity with respect to that sample, and the velocity ellipsoid that describes the peculiar motions of the sample. Each of these results is examined and compared to previous investigations. In the discussion, we use the $\sigma_k = 0.2$ results as our fiducial value, since it corresponds to $\sigma_{M_r} = 0.4$ which is observed for nearby stars with trigonometric parallaxes in the M_r, $r - z$ color–magnitude diagram.

4.1. Absolute Magnitudes

Traditionally, colors or spectral types have been employed to estimate absolute magnitude when trigonometric parallaxes were not available. These are often referred to as photometric and spectroscopic parallaxes, respectively. In Figure 2, we show the spectroscopic (left panel) and photometric (right panel) parallax relations for M dwarfs, compared to previous studies in the *ugriz* system (Hawley et al. 2002; West et al. 2005; Kraus & Hillenbrand 2007). The open circles are nearby low-mass stars with accurate trigonometric parallaxes, tabulated in Bochanski (2008). Using the Hammer (Covey et al. 2007), we manually assigned a spectral type to each nearby star, using archival spectra from multiple sources: the PMSU study (Reid et al. 1995; Hawley et al. 1996), SDSS, the local star sample of Cruz & Reid (2002), and the DwarfArchives Web site.[6] While many of the spectral types agreed with previous results, we did find some disagreements at the level of ±2 spectral classes. Therefore, we include updated spectral types for these nearby stars in Table 4. The left panel of Figure 2 highlights the large dispersion in M_r as a function of spectral type. The typical spread is ∼0.5 mag, increasing to ∼0.8 mag near type M4, nearly double the spread for a given $r-z$ color bin. Thus, we strongly suggest that spectral type should *not* be used as a tracer of absolute magnitude for M dwarfs. The use of half-integer spectral types may decrease the observed scatter in Figure 2. However, half-integer spectral types would require higher-resolution and higher signal-to-noise spectra, which is not practical for this type of large survey sample. Furthermore, half-integer spectral-type standards are not defined for the entire M dwarf sequence (Kirkpatrick et al. 1991). Finally, half-integer types will likely span a larger color range than the color bins we have used (see Paper I for a discussion of spectral types and mean colors).

The left panel of Figure 2 also displays disagreement between our statistical parallax results (solid black, red, and blue lines and filled circles) and the nearby star sample at later types. This is due to a systematic color difference within a given spectral-type bin between the two samples. That is, the nearby star sample is systematically redder than the SDSS stars at a given spectral type, possibly due to the small number of nearby stars in these bins. Thus, the SDSS stars have an absolute magnitude (at a given spectral type) that is appropriate for the bluer, more luminous stars of that type. This effect disappears when $r-z$ color is substituted for spectral type (Figure 2, right panel).

The right panel of Figure 2 shows our statistical parallax M_r, $r - z$ relation, along with the results of previous studies (Hawley et al. 2002; West et al. 2005; Bochanski et al. 2010). Overplotted with open circles are the absolute magnitudes and colors from the nearby star sample listed in Table 4. Note that the dispersion in absolute magnitude as a function of color is significantly smaller than that shown in left panel of Figure 2, indicating that the $r-z$ color is a much better tracer of absolute magnitude. Furthermore, the discrepancy in mean color for a given spectral type between the nearby star sample and SDSS stars is not evident. We reiterate that colors, rather than spectral types, are preferred for absolute magnitude and hence distance estimation for M dwarfs.

4.1.1. Absolute Magnitude Variations and Magnetic Activity

Due to the large spread in M_r as a function of spectral type, we focus our absolute magnitude analysis on our color

---

[6] Available at http://www.dwarfarchives.org.
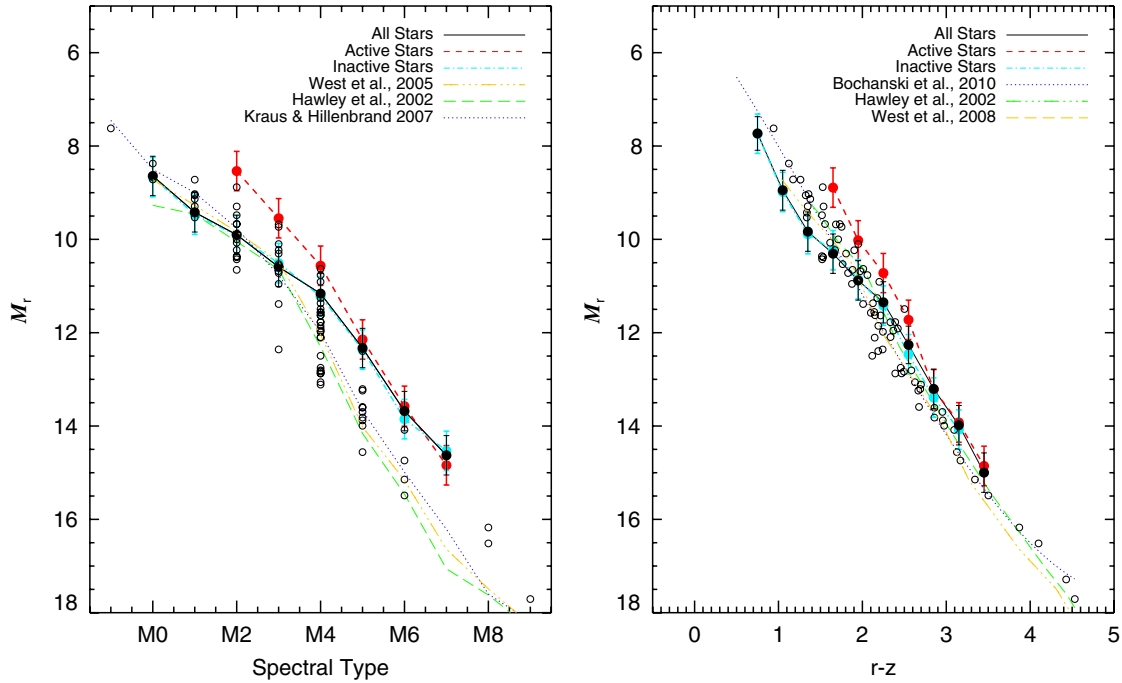
Figure 2. Left panel: M_r vs. spectral type. The open circles are nearby stars with accurate trigonometric parallaxes from Bochanski ([2008]). Previous spectroscopic parallax relations are overplotted and described in the legend. The results from this study (black, red, and blue lines and black filled circles) are plotted for comparison. Note the large dispersion in M_r for a given spectral type, especially at M4 and M5. We strongly suggest that spectral type should not be used to estimate absolute magnitude in the SDSS r band. Right panel: M_r vs. $r-z$, with same symbols and lines as in the spectral-type panel. Previous studies are shown and described in the legend. There is a much smaller dispersion in M_r at a given $r-z$ color compared to the spectral-type relations.

(A color version of this figure is available in the online journal.)

subsamples (i.e., the right panel of Figure 2). Our results are shown in the solid black, red, and blue lines and filled circles in Figure 2. There are a few notable trends. First, the bifurcated main sequence at blue colors (earlier spectral types) indicates that active, early-type M dwarfs are intrinsically more luminous than their inactive counterparts. Recent observations of eclipsing binaries (López-Morales [2007]; Morales et al. [2010]) and active, single stars (Berger et al. [2006]; Morales et al. [2008]) suggest that active stars possess larger radii than inactive dwarfs. However, possible changes in effective temperature and luminosity have not been well constrained. Models predict both unchanged (Chabrier et al. [2007]) or decreased (Mullan & MacDonald [2001]) luminosity, while some observations suggest that active low-mass dwarfs are overluminous compared to their model predictions (Mohanty et al. [2009]; Stelzer et al. [2010]). A similar effect was observed in the PMSU sample, where active M dwarfs were brighter in V than inactive stars (Figure 4 of Hawley et al. [1996]). The behavior evidenced in Figure 2 suggests that active, early-type M dwarfs are ~1 mag brighter in M_r, which could be explained if they have larger radii than inactive stars at the same spectral type or color. Direct interferometric measurements of stellar radii are necessary to independently quantify the amount the radius changes for an individual star, since our statistical analysis is performed on subsamples of stars that span a (small but nonzero) range of temperature. We note that many close binaries are unresolved in SDSS photometry. Binarity may increase activity in early M dwarfs in close orbits and could explain some of the absolute magnitude differences for those bins.

At blue colors ($r - z < 2$), the inactive and total sample absolute magnitudes fall below the mean locus of nearby trigonometric parallax stars. Since the nearby stars are composed of a mix of active and inactive stars, activity is likely not the only

important effect. We therefore next investigate the effects of metallicity on M_r and attempt to isolate them from those traced by chromospheric activity.

4.1.2. Absolute Magnitude Variations and Metallicity

While magnetic activity may affect the radius of a star, metallicity can alter the star's effective temperature and luminosity, manifesting as a change in absolute magnitude. At a given color (or spectral type), stars with lower metallicities will exhibit fainter absolute magnitudes (Sandage & Eggen [1959]; An et al. [2008]).[7] Without precise metallicities and trigonometric parallaxes for all the M dwarfs in our sample, we cannot directly examine this effect. There are some promising metallicity estimators for low-mass stars being developed in the near-IR (Johnson & Apps [2009]; Rojas-Ayala et al. [2010]), but these are not applicable to SDSS spectroscopy.

We therefore investigated the effects of metallicity using the ζ parameter, as defined by Lépine et al. ([2007]). ζ is a relative metallicity proxy which uses the relative strengths of CaH and TiO bands to discriminate between stars of different composition. It can be employed as a rough tracer of [Fe/H], with $\zeta = 1$ corresponding to solar metallicity and $\zeta = 0.4$ corresponding to [Fe/H] ~ -1 (Woolf et al. [2009]). We note that the [Fe/H]–ζ relation is only calibrated over spectral types M0–M3 and suffers from large spreads near solar metallicity. In Figure 3, we plot the absolute magnitudes for two bins in ζ as a function of spectral type (left panel) and $r-z$ color (right panel) for active (solid lines) and inactive (dashed lines) stars. Table 5 gives the M_r results for the various $r-z$, activity, and ζ bins. The spread in each bin is $\sigma \approx 0.4$ mag, set

---

[7] Alternatively, at a given mass, stars with lower metallicities are bluer (hotter) and more luminous than their high-metallicity counterparts.

Table 4
Nearby Star Sample Spectral Types

Name	α^a	δ^a	Sp. Type	Source[b]
GJ1002	1.67972278	−7.538550	M6	1
GJ1025	15.23465440	−4.449231	M5	1
Gl54.1	18.12784543	−16.998746	M5	1
LHS1302	27.76670103	−6.117972	M5	1
LHS1326	30.56747119	10.337209	M6	1
LHS1358	33.22773200	0.004801	M4	1
LHS1375	34.12457669	13.586802	M6	1
GL109	41.06474242	25.523168	M2	1
T832-10443	43.10949326	0.939522	M9	3
LHS168	48.34574221	4.774824	M5	1
GJ1065	57.68434297	−6.095079	M3	1
Gl169.1A	67.79870688	58.976686	M4	1
LHS1723	75.48913133	−6.946128	M4	1
G99-49	90.01463326	2.706515	M4	1
LHS1809	90.62144398	49.865368	M5	1
Gl232	96.17218963	23.432802	M4	1
Gl251	103.70407576	33.268001	M3	1
GJ1093	104.87030750	19.348539	M5	1
BL Lyn	112.98873721	36.229615	M4	1
2M0746+20	116.67677307	20.008842	L0	4
GJ1105	119.55303380	41.303596	M4	1
GJ2066	124.03289059	1.302435	M2	1
GJ1111	127.45563147	26.775994	M8	1
T213-2005	155.36376953	50.917938	L0	4
LHS283	158.86050669	69.449381	M4	1
Gl445	176.92332403	78.691261	M4	1
Gl447	176.93515470	0.804025	M4	1
GJ1151	177.73956422	48.377048	M4	1
GJ3693	178.46963501	6.998430	M8	2
Gl452.4	178.73946569	28.737442	K7	1
Gl455	180.57503136	28.587004	M3	1
GJ1156	184.74706541	11.126184	M6	1
Gl463	185.75015884	64.030910	M3	1
GJ1159A	187.30915386	53.545801	M4	1
LHS2633	191.75375224	46.625855	M2	1
Gl493.1	195.13932515	5.685628	M5	1
Gl514	202.49948063	10.376790	M1	1
Gl521	204.85046387	46.186687	M1	1
LHS2784	205.68017011	33.289742	M4	1
LHS2884	213.82055327	45.014702	M3	1
GJ3849	217.17973328	33.176899	L0	4
Gl552	217.37332947	15.533145	M2	1
GJ3855	217.65687658	59.723624	M8	4
Gl555	218.57030665	−12.519293	M4	1
2M1501+22	225.28405762	22.833836	M9	4
LHS3018	226.07657872	60.384562	M1	1
Gl581	229.86143531	−7.722272	M3	1
Gl585	230.96299622	17.465422	M4	1
LHS3080	232.97554057	28.852619	M4	1
Gl609	240.71170993	20.588769	M4	1
Gl625	246.35287094	54.304172	M2	1
Gl628	247.57513257	−12.662992	M4	1
LTT14949	250.20368457	36.316638	M2	1
GL643	253.85475375	−8.322944	M4	1
GJ1207	254.27401671	−4.349044	M4	1
LHS3262	255.84984701	51.406478	M4	1
GJ1209	256.09302479	16.931814	M3	1
Gl655	256.78099478	21.554112	M3	1
LTT15087	257.89507230	38.442849	M4	1
Gl678.1	262.59473243	5.548422	M0	1
Gl686	264.47272430	18.592155	M1	1
Gl694	265.98321814	43.378370	M2	1
GJ1223	270.69304642	37.517084	M5	1
Gl701	271.28155234	−3.031352	M1	1
Gl1227	275.61219859	62.049964	M5	1
Gl720B	278.86411519	45.761550	M4	1

Table 4
(Continued)

| Name	α^a	δ^a	Sp. Type	Source[b]
Gl725B	280.69435149	59.627614	M3	1
Gl729	282.45607171	−23.836125	M4	1
Gl745A	286.77322036	20.887782	M2	1
Gl745B	286.80506716	20.876758	M2	1
G207-22	288.12267278	35.564413	M2	1
Gl752A	289.22996750	5.168470	M3	1
GJ1235	290.41104011	20.867176	M4	1
GJ1253	306.52229530	58.573236	M5	1
Gl809	313.33253189	62.153943	M1	1
LHS3713	327.06371612	27.927964	M2	1
Gl849	332.41848642	−4.640774	M3	1
Gl127-35	337.19158157	18.931698	M0	1
Gl867B	339.68865820	−20.614020	M4	1
Gl867AC	339.68997030	−20.620763	M2	1
Gl908	357.30266119	2.400989	M1	1

Notes.
[a] α and δ are reported in decimal degrees and J2000 coordinates.
[b] (1) PMSU (Reid et al. 1995), (2) DwarfArchives.org, (3) SDSS (Paper I), and (4) Cruz & Reid (2002).

by the choice of $\sigma_k = 0.2$. As with any magnitude limited survey (such as SDSS), Malmquist (1936) bias can arise. For surveys with complicated selection effects, a magnitude-independent correction is preferred (Popowski & Gould 1998). For an exponential Galactic disk and $\sigma_{M_r} = 0.4$, the Malmquist correction is 0.15 mag (Reid & Hawley 2005). This correction has been applied to the values reported in Table 5 and is much smaller than the reported uncertainty.

Figure 3 demonstrates that for stars with similar chromospheric properties, the lower metallicity ones have fainter absolute magnitudes, at the same color or spectral type. This is consistent with cluster studies within the SDSS footprint (An et al. 2008) and trigonometric parallax studies of subdwarfs (Reid 1997). Active stars at the same metallicity are brighter than their inactive counterparts, but Figure 3 shows that both metallicity and activity are important for determining the luminosity of an individual star. At a fixed ζ, the difference in M_r is consistent with Figure 2, with early-type active stars being ∼1 mag brighter, and the difference diminishing at later spectral types. A similar offset was also measured for the same stars in M_g. The total SDSS sample is overplotted in each figure with a solid black line. The early-type stars, which are seen at larger distances due to SDSS magnitude limits (see Table 3), fall near the lower metallicity, inactive loci, while the later-type stars, seen closer to the Sun, are consistent with solar metallicities and active stars. This suggests that the low-mass dwarfs are tracing a metallicity gradient similar to the one observed in SDSS observations of higher-mass stars (Ivezić et al. 2008), and also explains why the SDSS sample falls below the locus of nearby stars at early types (right panel of Figure 2).

We also note that the activity–metallicity loci appear to converge near M5 ($r − z \sim 2.8$). This behavior is not well explained, but may be linked to the transition between a partially and fully convective stellar interior that occurs near that spectral type/color. Perhaps this transition, which alters the efficiency of energy transport in the star, also regulates the luminosity at the surface.

Finally, we examined the IPA and hemisphere subsamples. No significant differences were observed in the spectroscopic or photometric parallax relations with respect to position in
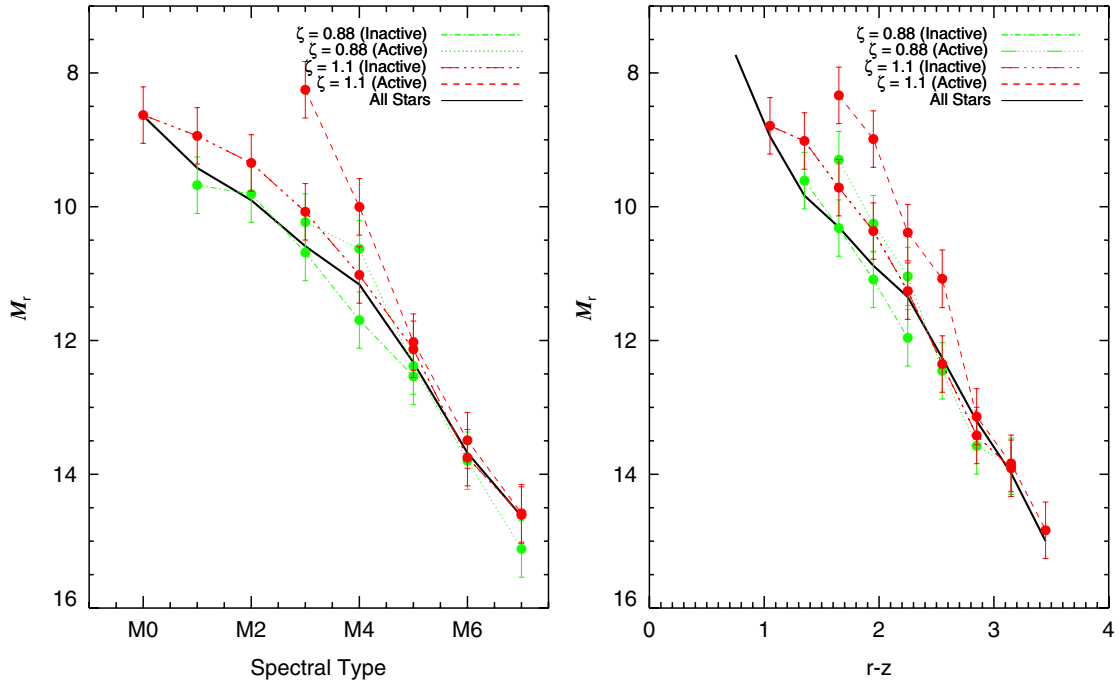
Figure 3. Left panel: M_r vs. spectral type for two values of ζ, a metallicity proxy. Active stars (dashed and dotted lines) and inactive stars (dot-dashed lines) at the same metallicity are plotted. The total sample is overplotted in the solid black line. At a given metallicity, active stars are brighter than their inactive counterparts, while low-metallicity stars ($\zeta = 0.88$) are dimmer than higher metallicity M dwarfs ($\zeta = 1.1$) at the same spectral type and activity state. Right panel: the M_r vs. $r-z$ results show the same features as in the spectral-type panel.

(A color version of this figure is available in the online journal.)

Table 5
Absolute Magnitudes of SDSS M Dwarfs

$r - z$	$\zeta = 1.1$		$\zeta = 0.88$	
	Active	Inactive	Active	Inactive
1.05	. . .	8.8	. . .	. . .
1.35	. . .	9.1	. . .	9.7
1.65	8.4	9.8	9.3	10.4
1.95	9.0	10.4	10.3	11.1
2.25	10.3	11.3	11.1	12.0
2.55	11.2	12.4	12.5	. . .
2.85	13.2	13.5	13.6	. . .
3.15	13.9	14.0	13.9	. . .
3.45	14.9	. . .	. . .	. . .

Notes. The typical uncertainty for the reported absolute magnitudes is $\sigma_{M_r} = 0.42$, which is directly computed from Equation (1).

Table 6
Solar Peculiar Motion

Study	$U_\odot$[a]	$V_\odot$[a, b]	$W_\odot$[a]
Hawley et al. ([1996](#))	9.1 ± 2	23.3 ± 2	7.6 ± 2
Dehnen & Binney ([1998](#))	10.00 ± 0.36	5.25 ± 0.62	7.17 ± 0.38
Dehnen & Binney ([1998](#))[c]	10 ± 1	22 ± 1	8 ± 2
Fuchs et al. ([2009](#))	9 ± 1	20 ± 2	7 ± 1
Aumer & Binney ([2009](#))	9.96 ± 0.33	5.25 ± 0.54	7.07 ± 0.34
Bond et al. ([2010](#))	10[d]	20	6.5 ± 0.4
Schönrich et al. ([2010](#))	11.1 ± 1	12.24 ± 2	7.25 ± 0.5
This study[e]	8 ± 2	24 ± 3	7 ± 2

Notes.
[a] *UVW* velocities are reported in km s^{-1}, with U increasing radially inward, V increasing in the direction of the solar orbit, and W increasing above the Galactic plane.
[b] Measured relative to nearby M dwarfs, except for the Dehnen & Binney ([1998](#)) and Aumer & Binney ([2009](#)) studies.
[c] Estimated from reddest bin in Figure 3 of Dehnen & Binney ([1998](#)).
[d] Assumed.
[e] Error-weighted mean over spectral types M0–M7.

the Galaxy. A trend with IPA was expected, since this proxy for height probably traces metallicity. The lack of a gradient is probably due to stars at various heights being scattered into the same IPA bin due to photometric errors. The agreement between the hemisphere subsamples indicates that the extinction correction is adequate for the sample.

4.2. Kinematics of M Dwarfs

In addition to an absolute magnitude estimate, the analysis returns kinematic information for each subsample. The interpretation of the kinematic results is complicated by the disjoint spatial volumes that the samples inhabit (see Table 3). We discuss the mean motions of M dwarfs as traced by the solar reflex motion, the velocity dispersions exhibited by active stars compared to their inactive counterparts, and the change in velocity dispersions seen in samples at different galactic heights.

4.2.1. Solar Peculiar Motion

The statistical parallax method measures the reflex solar motion with respect to the mean velocity of the stellar subsample being analyzed. If subsamples possess different mean velocities, this will be manifested as a change in the solar reflex motion. For reference, we use a coordinate system with U increasing toward the Galactic center, V increasing in the direction of solar motion, and W increasing vertically upward (as in Dehnen & Binney [1998](#)). This system is right handed, with the angular momentum vector of the solar orbital motion pointing toward the south Galactic pole.
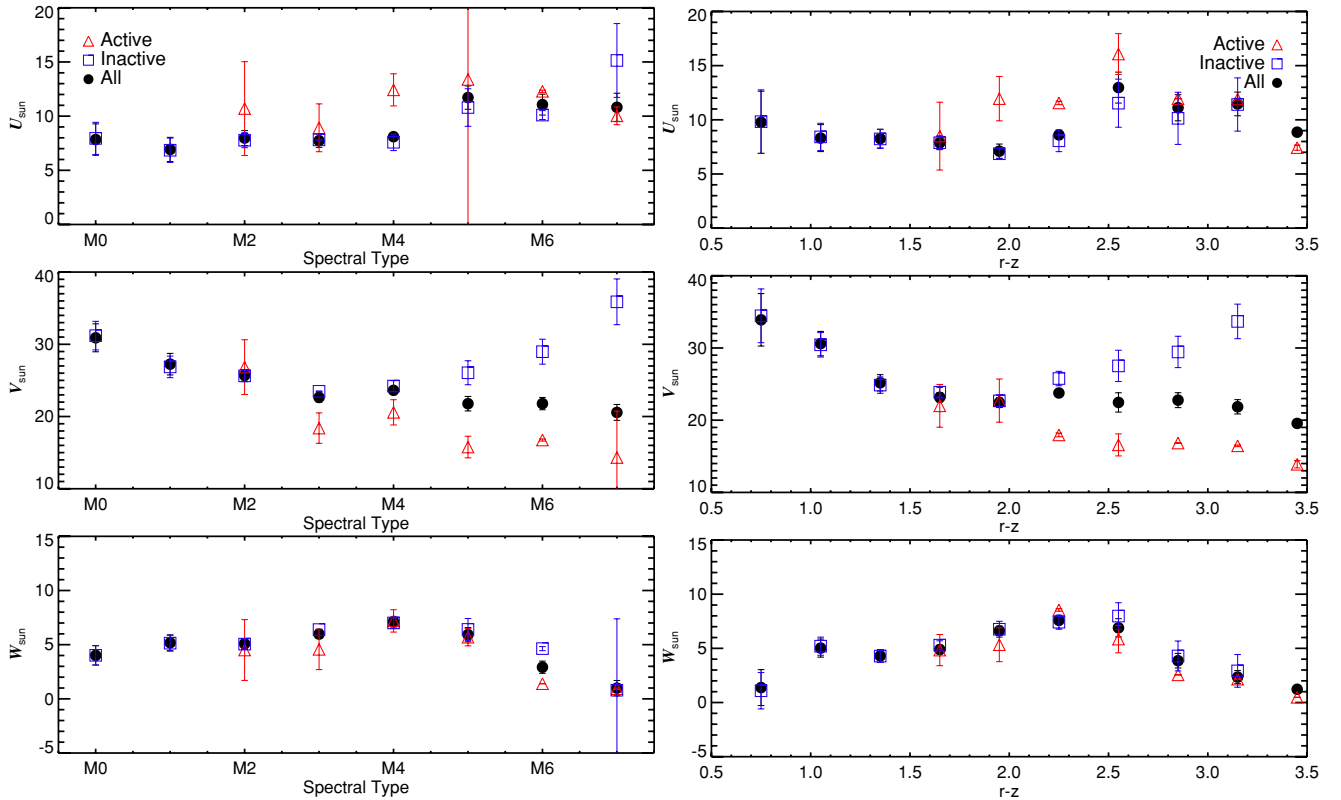
Figure 4. Solar peculiar motion as a function of spectral type (left panel) and $r-z$ color (right panel). The V velocities exhibit a decline to later type (or redder) stars, likely due to an age effect, as shown by the separation between the active and inactive populations. The W velocities exhibit a peaked behavior, while the U velocities show a rise toward later types, which occurs at a bluer color in the active population.

(A color version of this figure is available in the online journal.)

In the U and W directions, the solar reflex motion reflects the Sun's peculiar motion, as these distributions should be centered on the local standard of rest (LSR; Fuchs et al. 2009). The solar reflex motion in the V direction is a combination of the Sun's peculiar motion and the asymmetric drift at the solar circle (Strömberg 1924, 1925). This shifts the mean V velocity of a sample of typical disk-age M dwarfs, giving a V reflex motion larger than one measured from a population of young stars. Our results are shown in Figure 4, and we compare our peculiar solar velocities (i.e., the negative of the reflex motion) to previous work in Table 6. Our values were computed by taking the weighted mean across all spectral types with the uncertainty given by the standard deviation. While the U and W velocities remain relatively constant with spectral type, the V reflex motion is significantly larger at early spectral types (M0–M2). These stars are observed at larger distances (Table 3) and also have larger velocity dispersions (as seen in Figure 6). The same behavior is observed for the bluest $r-z$ colors, which contain the same early-type M stars. For $r-z > 2$, the V velocity of the Sun remains relatively constant at 20 km s^{-1}. This value compares favorably to the V velocities derived by Hawley et al. (1996) and Fuchs et al. (2009), both measured with M dwarfs, but is larger than the $V \sim 5$ km s^{-1} value reported by Dehnen & Binney (1998) from measurements of the Sun's motion through a very young population, due to the age range of the stars that populate our subsamples. At later types, where the separation in age is most extreme between the active and inactive populations (see West et al. 2008, and discussion in Section 4.2.2 below), the active stars in the sample show decreasing V velocities, while the inactive stars have increasing V velocities, which supports the age hypothesis.

As mentioned above, the measured solar reflex velocity is the relative motion between the Sun and the mean velocity of a subsample of M dwarfs.[8] Since the Sun's velocity is not changing, a measured change in the reflex velocity indicates a difference in the mean velocity of a particular subsample with respect to the LSR. While the U and W velocity dispersions are expected to be constant with color (or spectral type), we find that there is significant structure in both distributions. The W velocity distribution in Figure 4 displays a non-monotonic behavior, peaking near $r - z \sim 2.3$ (type M4). This structure indicates that the mean vertical motion of the particular M dwarf subsample is varying, with both bluer and redder M dwarfs having a smaller mean velocity. The W velocities of active and inactive stars are not significantly different. Meanwhile, the U velocity distribution shows a different behavior, remaining relatively constant from M0 to M5 ($r - z \sim 2.5$), and then exhibiting a rise toward later types. The active stars appear to show this rise in U velocity at a bluer color ($r-z \sim 2.0$), but then are joined by the inactive stars at later types. This may be due to the changes seen in the other (V, W) velocities and/or to the change in the absolute magnitude of the active stars in bins where they are a significant fraction of the total distribution. Modeling of the populations to explore changing the various parameters (activity fraction, absolute magnitude, input velocities in each direction) is necessary in order to disentangle these related effects.

---

[8] We note that the solar motion has also been estimated by observing the direction and velocity of interstellar He entering the heliosphere (Witte 2004).
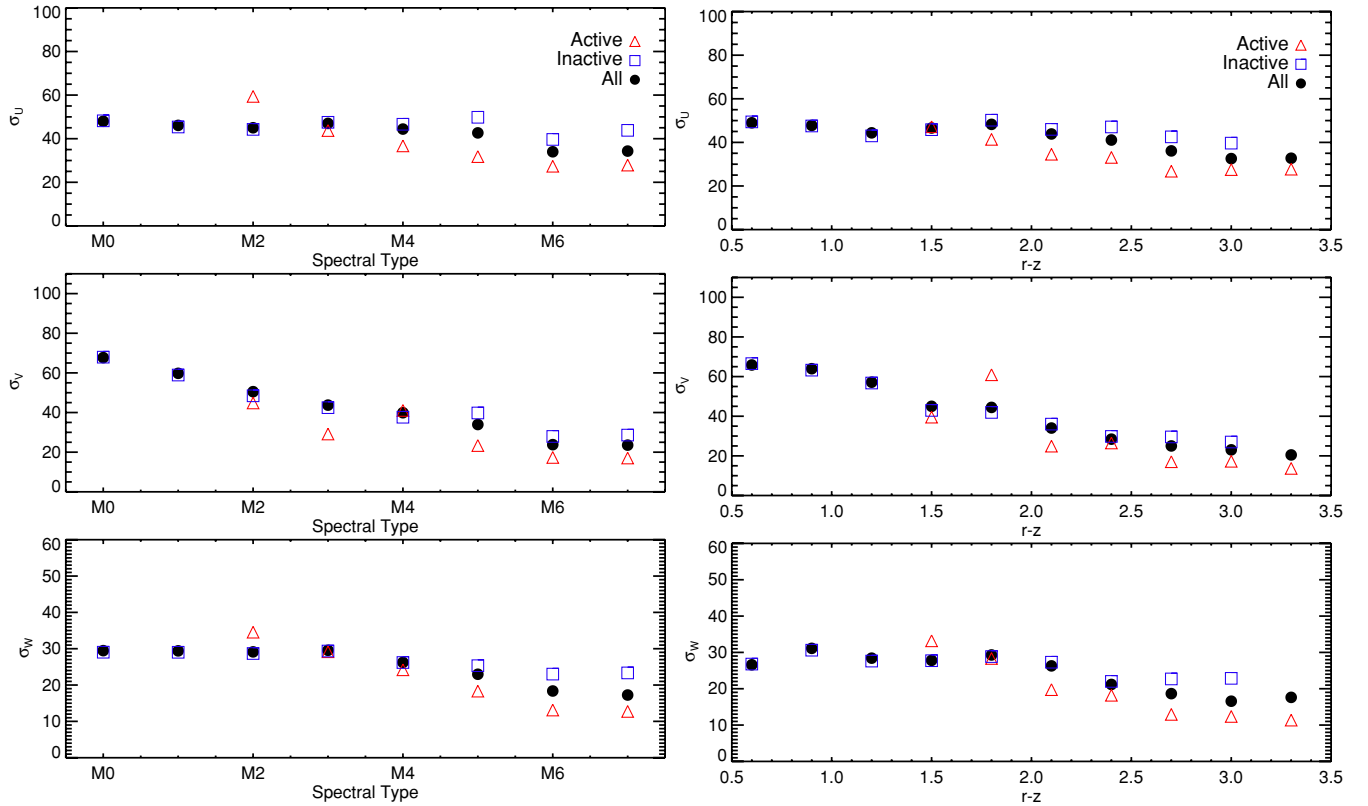
Figure 5. UVW velocity dispersions vs. spectral type (left panel) and color (right panel) for active (red triangles), inactive (blue squares), and all stars (filled black circles). Active stars possess smaller dispersions at mid-late spectral types (red colors). The M2 bin shows a strong vertex deviation, so the velocity dispersions should not be interpreted as measurements along the UVW axes.

(A color version of this figure is available in the online journal.)

Table 7
Velocity Dispersions of M dwarfs

| Spectral Type	σ_U (km s^{-1})			σ_V (km s^{-1})			σ_W (km s^{-1})		
	Active	Inactive	All	Active	Inactive	All	Active	Inactive	All
M0	. . .	48	47	. . .	67	67	. . .	29	29
M1	. . .	45	46	. . .	58	59	. . .	29	29
M2	59	44	45	44	66	48	34	28	29
M3	43	47	47	29	51	42	29	29	29
M4	36	46	44	41	41	37	24	26	26
M5	31	49	42	23	39	39	18	25	22
M6	27	39	33	17	28	27	13	23	18
M7	27	43	34	17	29	28	12	23	17
$r-z$									
0.75	. . .	49	48	. . .	66	65	. . .	26	26
1.05	. . .	47	47	. . .	63	63	. . .	30	31
1.35	. . .	42	44	. . .	56	57	. . .	27	28
1.65	47	45	46	39	42	44	33	27	27
1.95	41	50	48	60	41	44	28	28	29
2.25	34	45	43	24	36	34	19	27	26
2.55	33	47	41	26	29	28	18	22	21
2.85	26	42	36	17	29	25	12	22	18
3.15	27	39	32	17	26	23	12	22	16
3.45	27	. . .	32	13	. . .	20	11	. . .	17

Notes. The typical uncertainty for the dispersions is 5–10 km s^{-1} (Equation (1)).

4.2.2. Velocity Dispersions

The active M dwarfs are known to form a kinematically colder population than their inactive counterparts (e.g., Wielen 1977; Hawley et al. 1996), as evidenced by smaller velocity disper-

sions. This is usually interpreted as an age effect, where younger M dwarfs have had less time to interact with giant molecular clouds and spiral density waves. The velocity dispersion is predicted to vary as the square root of age (e.g., Fuchs et al. 2001; Hänninen & Flynn 2002). Young stars also harbor strong magnetic fields that heat their chromospheres, allowing activity to be used as a proxy for age (Wilson & Woolley 1970). Activity in low-mass stars has been shown to depend on both spectral type and age; inactive, late-type M dwarfs are usually much older than inactive early-type M dwarfs (West et al. 2008). In Table 7, we list the UVW velocity dispersions for the active and inactive subsamples by spectral type and color. Figure 5 shows the results. As expected, the dispersions of active stars separate from their inactive counterparts at the same spectral type (color) for mid-late M dwarfs. In the first bin where there are enough active stars to carry out the statistical parallax analysis (at spectral type M2), the active stars have larger reported dispersions than the inactive ones. The velocity ellipsoid in this case shows a strong vertex deviation, indicating a young population, which has not undergone significant dynamical heating (Binney & Merrifield 1998), and the velocity dispersions should not be interpreted as measurements along the UVW axes. The active M2 stars being members of a young population are consistent with age–activity relations that predict short activity lifetimes for early-type M stars. (West et al. 2008).

Another notable feature of Figure 5 is the decline in velocity dispersion at later types. Since the type (color) bins sample different spatial volumes (see Table 3), this is likely showing that stars that are located further above the plane of the Galaxy (in the early-type bins) are there because they are
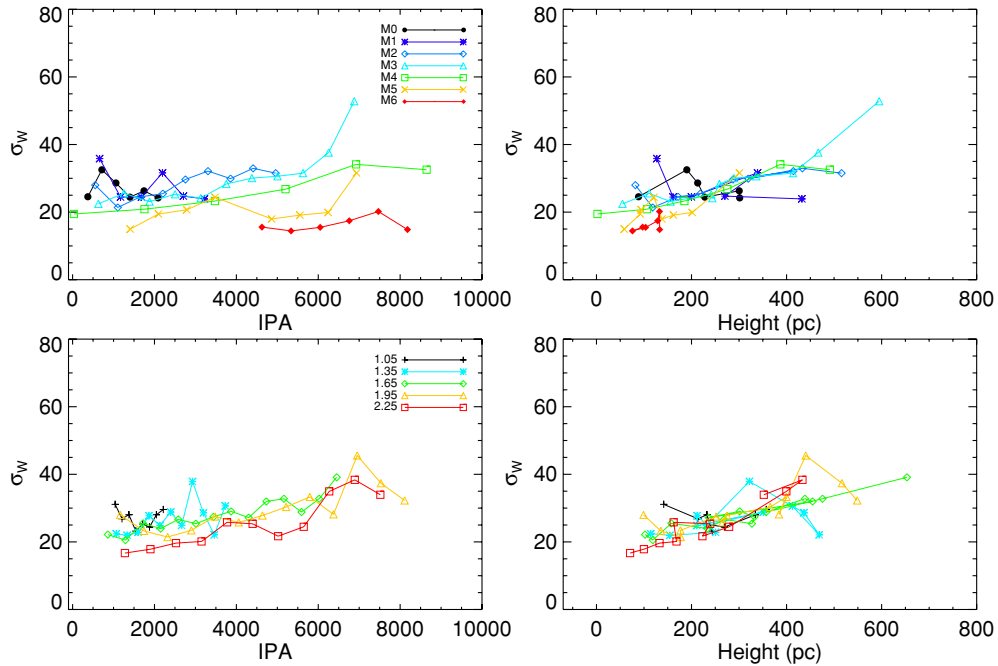
Figure 6. *W* velocity dispersions vs. IPA (left panels) and height above the plane (right panels). The velocity dispersions increase with IPA/height but do not depend on color/spectral type.

(A color version of this figure is available in the online journal.)

Table 8
Heights for Various IPAs and Absolute Magnitudes[a]

IPA	M_r			
	8	10	12	14
100	25	10	3	1
1000	251	100	39	15
3000	753	300	119	47
5000	1255	500	199	79
6000	1507	600	238	95

Note. [a] All heights reported in parsecs.

older and have undergone more dynamical interactions, giving correspondingly larger velocity dispersions. To investigate this kinematic structure in the Milky Way, we use the IPA parameter described in Equation (3) as a proxy for height.

The mean height above the Plane, z, can be approximated as

$$Z \approx d \sin b, \qquad (4)$$

where b is the mean Galactic latitude for the subsample ($\sim 50°$ for SDSS as a whole). This approximation neglects effects due to the Sun's location above the plane (15 pc; Cohen 1995), but see Bochanski et al. (2010) for a more precise expression. Given the definition of IPA in Equation (3), z and IPA are thus related by

$$Z \approx \text{IPA} 10^{(1 - \frac{M_r}{5})}. \qquad (5)$$

For reference, we tabulate various heights for a given IPA and M_r in Table 8. To increase the number of stars in each IPA bin, we used stars at the same absolute distance from the Plane in both the northern and southern Galactic hemispheres, thus implicitly assuming that the Galaxy is symmetric about its mid-plane.

Previous kinematic investigations (Bochanski et al. 2005, 2007a; West et al. 2008; Fuchs et al. 2009; Schmidt et al. 2010) have demonstrated an increase in velocity dispersion at

larger Galactic heights, rising from $(\sigma_U, \sigma_V, \sigma_W) \approx (30 \, \text{km s}^{-1}, 20 \, \text{km s}^{-1}, 20 \, \text{km s}^{-1})$ in the local solar neighborhood to $(\sigma_U, \sigma_V, \sigma_W) \approx (50 \, \text{km s}^{-1}, 40 \, \text{km s}^{-1}, 40 \, \text{km s}^{-1})$ at 1 kpc. In Figure 6, we plot the vertical W velocity dispersion as a function of IPA (left panels) and mean height above the Plane (right panels), for spectral type (upper row) and color (lower row). Recall that the advantage of the IPA is that no absolute magnitude is assumed, while the heights are calculated using the absolute magnitude from the statistical parallax solution for a given subsample. The increase in velocity dispersion is seen in both height and IPA. Furthermore, there is no strong dependence on spectral type or color, as expected since the dynamical interactions should be controlled by the Galactic gravitational potential, with the stars (of any mass) acting as collisionless test particles. These results bridge the gap between the kinematic investigations of Bond et al. (2010), which examined stars beyond our distances limits, and those examining nearby stars interior to our study (Nordström et al. 2004; Reid et al. 2002).

The velocity dispersions for M dwarfs listed in Table 7 should be interpreted in light of these IPA/height results. Earlier spectral types (i.e., M0 and M1) sample a larger range of distances and have a larger mean distance than later types (see Table 3). Figure 6 shows that both early-type and late-type M dwarfs have similar velocity dispersions when sampled at the same Galactic height.

5. CONCLUSIONS

We present a statistical parallax analysis of the most recent catalog of M dwarfs identified with SDSS spectroscopy (Paper I). Our sample was subdivided on many criteria, to explore both the intrinsic changes in low-mass dwarfs due to metallicity and magnetic activity, and to investigate their kinematics. We have demonstrated that $r - z$ color is a much better proxy for absolute magnitude than spectral type, and suggest that photometric parallaxes are the preferred method to determine absolute magnitudes and distances for M dwarfs.

Some interesting trends with M_r were revealed in our analysis. First, magnetically active M dwarfs were shown to be intrinsically brighter at the same spectral type or color than their inactive counterparts. Eclipsing binary studies have demonstrated that magnetic activity inflates a star's radius (Ribas 2006; López-Morales 2007; Morales et al. 2008, 2010), but the effect on effective temperature and luminosity is less constrained. Our results suggest that activity may increase the radius and luminosity of active low-mass stars.

Metallicity, which influences the luminosity of a star, was also explored. We divided the sample using the ζ parameter (Lépine et al. 2007) as a proxy for metallicity. Our results are similar to those observed for higher-mass stars: low-metallicity M dwarfs are dimmer at a given spectral type (or color) than high-metallicity stars. We have quantified this effect for M dwarfs in the SDSS photometric system.

To isolate the effects of metallicity and activity, we separated active and inactive stars for the same ζ as a function of color and spectral type. Activity still brightened stars at the same ζ, however the effect diminished at smaller ζ (lower metallicity).

The statistical parallax analysis also allowed us to investigate the reflex solar motion and velocity dispersions for each subsample. The more distant, early-type stars, which are presumably older, have the largest reflex solar motion, particularly in the V direction, which we attribute to the increased asymmetric drift. The active and inactive stars exhibit expected behavior with the active star populations having smaller mean motions relative to the Sun. The inactive, late-type M dwarfs, which we identify as an older population due to their lack of activity (ages $\gtrsim$ 4 Gyr; West et al. 2008) have velocity dispersions similar to early-type M dwarfs, which we identify as old due to their greater vertical distance from the Galactic plane. Thus, the activity and dynamical heating age indicators give consistent results. When the velocity dispersions are analyzed as a function of vertical height or IPA, all stars exhibit increasing dispersion at increasing height above the Plane.

As astronomy enters a new era of large photometric surveys, such as PanSTARRS (Kaiser et al. 2002) and LSST (Ivezic et al. 2008), it will be vital to develop techniques for estimating the activity and metallicity of low-mass stars from photometry alone. There have already been efforts to characterize metallicity using the color–color distributions of M dwarfs in SDSS (Lépine 2009; Paper I), but those data must be calibrated with spectroscopic observations. The work presented in this paper highlights the need to determine these fundamental parameters, since they affect the estimated distance to each star. Finally, the importance of the dual spectroscopic and photometric nature of SDSS cannot be overstated. The large spectroscopic samples of M dwarfs it has acquired have enabled many novel investigations, including this one. Significant spectroscopic follow-up of the next generation of surveys should be a high priority.

REFERENCES

Abazajian, K. N., et al. 2009, ApJS, 182, 543
An, D., et al. 2008, ApJS, 179, 326
Aumer, M., & Binney, J. J. 2009, MNRAS, 397, 1286
Berger, D. H., et al. 2006, ApJ, 644, 475
Bilir, S., Karaali, S., Ak, S., Coşkunoğlu, K. B., Yaz, E., & Cabrera-Lavers, A. 2009, MNRAS, 396, 1589
Binney, J., & Merrifield, M., (ed.) 1998, Galactic Astronomy (Princeton, NJ: Princeton Univ. Press), 636
Bochanski, J. J., Jr. 2008, PhD thesis, Univ. Washington
Bochanski, J. J., Hawley, S. L., Covey, K. R., West, A. A., Reid, I. N., Golimowski, D. A., & Ivezić, Ž. 2010, AJ, 139, 2679
Bochanski, J. J., Hawley, S. L., Reid, I. N., Covey, K. R., West, A. A., Tinney, C. G., & Gizis, J. E. 2005, AJ, 130, 1871
Bochanski, J. J., Munn, J. A., Hawley, S. L., West, A. A., Covey, K. R., & Schneider, D. P. 2007a, AJ, 134, 2418
Bochanski, J. J., West, A. A., Hawley, S. L., & Covey, K. R. 2007b, AJ, 133, 531
Bond, N. A., et al. 2010, ApJ, 716, 1
Chabrier, G., Gallardo, J., & Baraffe, I. 2007, A&A, 472, L17
Clube, S. V. M., & Jones, D. H. P. 1971, MNRAS, 151, 231
Cohen, M. 1995, ApJ, 444, 874
Covey, K. R., et al. 2007, AJ, 134, 2398
Covey, K. R., et al. 2008, AJ, 136, 1778
Cruz, K. L., & Reid, I. N. 2002, AJ, 123, 2828
Dahn, C. C., et al. 2002, AJ, 124, 1170
Daniels, R. 1978, Introduction to Numerical Methods and Optimization Techniques (New York: North-Holland)
Davenport, J. R. A., Bochanski, J. J., Covey, K. R., Hawley, S. L., West, A. A., & Schneider, D. P. 2007, AJ, 134, 2430
Dehnen, W., & Binney, J. J. 1998, MNRAS, 298, 387
Dhital, S., West, A. A., Stassun, K. G., & Bochanski, J. J. 2010, AJ, 139, 2566
ESA 1997, VizieR Online Data Catalog, 1239, 0
Fernley, J., Barnes, T. G., Skillen, I., Hawley, S. L., Hanley, C. J., Evans, D. W., Solano, E., & Garrido, R. 1998, A&A, 330, 515
Fuchs, B., Dettbarn, C., Jahreiß, H., & Wielen, R. 2001, in ASP Conf. Ser. 228, Dynamics of Star Clusters and the Milky Way, ed. S. Deiters, B. Fuchs, A. Just, R. Spurzem, & R. Wielen (San Francisco, CA: ASP), 235
Fuchs, B., et al. 2009, AJ, 137, 4149
Fukugita, M., Ichikawa, T., Gunn, J. E., Doi, M., Shimasaku, K., & Schneider, D. P. 1996, AJ, 111, 1748
Hänninen, J., & Flynn, C. 2002, MNRAS, 337, 731
Hawley, S. L., Gizis, J. E., & Reid, I. N. 1996, AJ, 112, 2799
Hawley, S. L., Jefferys, W. H., Barnes, T. G., III, & Lai, W. 1986, ApJ, 302, 626
Hawley, S. L., et al. 2002, AJ, 123, 3409
Ivezic, Z., et al. 2008, arXiv:0805.2366
Ivezić, Z., et al. 2008, ApJ, 684, 287
Johnson, J. A., & Apps, K. 2009, ApJ, 699, 933
Jurić, M., et al. 2008, ApJ, 673, 864

Kaiser, N., et al. 2002, Proc. SPIE, 4836, 154
Kirkpatrick, J. D., Henry, T. J., & McCarthy, D. W. 1991, ApJS, 77, 417
Kraus, A. L., & Hillenbrand, L. A. 2007, ApJ, 662, 413
Laughlin, G., Bodenheimer, P., & Adams, F. C. 1997, ApJ, 482, 420
Layden, A. C., Hanson, R. B., Hawley, S. L., Klemola, A. R., & Hanley, C. J. 1996, AJ, 112, 2110
Lépine, S. 2009, in AIP Conf. Ser. 1094, Cool Stars, Stellar Systems, and the Sun: Proc. 15th Cambridge Workshop on Cool Stars, Stellar Systems, and the Sun, ed. E. Stempels (Melville, NY: AIP), 545
Lépine, S., Rich, R. M., & Shara, M. M. 2007, ApJ, 669, 1235
Lépine, S., Thorstensen, J. R., Shara, M. M., & Rich, R. M. 2009, AJ, 137, 4109
López-Morales, M. 2007, ApJ, 660, 732
Luyten, W. J. 1925, ApJ, 62, 8
Malmquist, K. G. 1936, Stockholm Obs. Medd., 26
Mohanty, S., Stassun, K. G., & Mathieu, R. D. 2009, ApJ, 697, 713
Morales, J. C., Gallardo, J., Ribas, I., Jordi, C., Baraffe, I., & Chabrier, G. 2010, ApJ, 718, 502
Morales, J. C., Ribas, I., & Jordi, C. 2008, A&A, 478, 507
Mullan, D. J., & MacDonald, J. 2001, ApJ, 559, 353
Munn, J. A., et al. 2004, AJ, 127, 3034
Munn, J. A., et al. 2008, AJ, 136, 895
Murray, C. A. (ed.) 1983, Vectorial Astrometry
Nelder, J. A., & Mead, R. 1965, Comput. J., 7, 308
Nordström, B., et al. 2004, A&A, 418, 989
Perryman, M. A. C., et al. 2001, A&A, 369, 339
Pier, J. R., Munn, J. A., Hindsley, R. B., Hennessy, G. S., Kent, S. M., Lupton, R. H., & Ivezić, Ž. 2003, AJ, 125, 1559
Popowski, P., & Gould, A. 1998, ApJ, 506, 259
Reid, I. N. 1997, AJ, 114, 161
Reid, I. N., Gizis, J. E., Cohen, J. G., Pahre, M. A., Hogg, D. W., Cowie, L., Hu, E., & Songaila, A. 1997, PASP, 109, 559
Reid, I. N., Gizis, J. E., & Hawley, S. L. 2002, AJ, 124, 2721
Reid, I. N., & Hawley, S. L. (ed.) 2005, New Light on Dark Stars Red Dwarfs, Low-Mass Stars, Brown Stars (Springer-Praxis Books in Astrophysics and Astronomy; Chichester: Praxis Publishing Ltd.)

Reid, I. N., Hawley, S. L., & Gizis, J. E. 1995, AJ, 110, 1838
Reid, N., & Majewski, S. R. 1993, ApJ, 409, 635
Ribas, I. 2006, Ap&SS, 304, 89
Richards, G. T., et al. 2002, AJ, 123, 2945
Riedel, A. R., et al. 2010, AJ, 140, 897
Rojas-Ayala, B., Covey, K. R., Muirhead, P. S., & Lloyd, J. P. 2010, ApJ, 720, L113
Sandage, A. R., & Eggen, O. J. 1959, MNRAS, 119, 278
Schlegel, D. J., Finkbeiner, D. P., & Davis, M. 1998, ApJ, 500, 525
Schmidt, S. J., West, A. A., Hawley, S. L., & Pineda, J. S. 2010, AJ, 139, 1808
Schönrich, R., Binney, J., & Dehnen, W. 2010, MNRAS, 403, 1829
Sesar, B., Ivezić, Ž., & Jurić, M. 2008, ApJ, 689, 1244
Skrutskie, M. F., et al. 2006, AJ, 131, 1163
Smart, R. L., Ioannidis, G., Jones, H. R. A., Bucciarelli, B., & Lattanzi, M. G. 2010, A&A, 514, A84
Stelzer, B., Scholz, A., Argiroffi, C., & Micela, G. 2010, MNRAS, 408, 1095
Strauss, M. A., et al. 2002, AJ, 124, 1810
Strömberg, G. 1924, ApJ, 59, 228
Strömberg, G. 1925, ApJ, 61, 363
Strugnell, P., Reid, N., & Murray, C. A. 1986, MNRAS, 220, 413
van Herk, G. 1965, Bull. Astron. Inst. Neth., 18, 71
van Leeuwen, F. 2007, A&A, 474, 653
Vrba, F. J., et al. 2004, AJ, 127, 2948
West, A. A., Hawley, S. L., Bochanski, J. J., Covey, K. R., Reid, I. N., Dhital, S., Hilton, E. J., & Masuda, M. 2008, AJ, 135, 785
West, A. A., Walkowicz, L. M., & Hawley, S. L. 2005, PASP, 117, 706
West, A. A., et al. 2011, AJ, 141, 97
Wielen, R. 1977, A&A, 60, 263
Wilson, O., & Woolley, R. 1970, MNRAS, 148, 463
Wilson, T. D., Barnes, T. G., III, Hawley, S. L., & Jefferys, W. H. 1991, ApJ, 378, 708
Witte, M. 2004, A&A, 426, 835
Woolf, V. M., Lépine, S., & Wallerstein, G. 2009, PASP, 121, 117
York, D. G., et al. 2000, AJ, 120, 1579